Crystal structure of the clathrin adaptor protein 1 core

Ekaterina E. Heldwein*, Eric Macia[†‡§], Jing Wang[§¶], Helen L. Yin[¶], Tomas Kirchhausen[†‡], and Stephen C. Harrison*[‖]**

*Children's Hospital, [‖]Howard Hughes Medical Institute, [†]Department of Cell Biology, and [‡]CBR Institute for Biomedical Research, Harvard Medical School, Boston, MA 02115; and [¶]Department of Physiology, University of Texas Southwestern Medical Center, Dallas, TX 75390

Contributed by Stephen C. Harrison, August 19, 2004

The heterotetrameric adaptor proteins (AP complexes) link the outer lattice of clathrin-coated vesicles with membrane-anchored cargo molecules. We report the crystal structure of the core of the AP-1 complex, which functions in the trans-Golgi network (TGN). Packing of complexes in the crystal generates an exceptionally long (1,135-Å) unit-cell axis, but the 6-fold noncrystallographic redundancy yields an excellent map at 4-Å resolution. The AP-1 core comprises N-terminal fragments of the two large chains, β1 and γ, and the intact medium and small chains, μ1 and σ1. Its molecular architecture closely resembles that of the core of AP-2, the plasma-membrane-specific adaptor, for which a structure has been determined. Both structures represent an ''inactive'' conformation with respect to binding of cargo with a tyrosine-based sorting signal. TGN localization of AP-1 depends on the small GTPase, Arf1, and the phosphoinositide, PI-4-P. We show that directed mutations of residues at a particular corner of the γ chain prevent recruitment to the TGN in cells and diminish PI-4-P-dependent, but not Arf1-dependent, liposome binding *in vitro*.

Clathrin-coated vesicles carry molecular cargo between intracellular membrane-bound compartments. Clathrin is the framework for assembly of a vesicular coat; loading of cargo into nascent coated vesicles (''coated pits'') requires one or more adaptor proteins (APs), which interact with both the clathrin lattice and the cargo molecule. An important group of clathrin adaptors are the heterotetrameric AP complexes, assemblies of two related but distinct ''large chains,'' a medium chain, and a small chain. Mammalian cells have four such heterotetrameric APs, designated AP-1 through AP-4, each of which works in a particular traffic route: AP-1 (γ, β1, μ1, and σ1), AP-3 (δ, β3, μ3, and σ3), and AP-4 (ε, β4, μ4, and σ4) in the trans-Golgi network (TGN) and endosomes and AP-2 (α, β2, μ2, and σ2) at the plasma membrane (for reviews, see refs. 1–3).

Membrane-anchored cargo molecules interact with adaptors through short ''sorting signals'' in their cytosolic segments. For example, a number of important membrane proteins, such as transferrin receptor and Lamp-1, are sorted through engagement of a YppΦ sequence with the μ2 and μ1 chains of AP-2 and AP-1, respectively (where Y is tyrosine; p, a polar residue; and Φ, a bulky hydrophobic residue). The heterotetrameric APs have a ''core'' and two ''appendages.'' The core comprises the two ≈70-kDa N-terminal domains (''trunks'') of the large chains, the ≈50-kDa μ chain, and the ≈20-kDa σ chain. The appendages are C-terminal domains of each of the large chains, connected to the rest of the structure by extended hinge segments. The structure of the AP-2 core has been determined by Owen and coworkers (4). The trunks of the large chains create a hollow socket, into which insert the σ2 chain and the N-terminal domain of the μ2 chain (μ2N). The C-terminal domain of μ2 (μ2C) forms a concave platform across one face of the assembly. Its link to μ2N is a flexible and partly disordered segment of ≈20 residues. Recognition of YppΦ endocytic signals occurs on μ2C, as shown by crystal structures of the isolated domain in complex with sorting-signal peptides (5). The binding site is partly blocked in the intact core by the way the μ2 platform docks against the β chain. Collins *et al.* (4) have suggested that their core structure represents an inactive state, and that activation requires an outward displacement of μ2C to expose the contact site.

Localization of heterotetrameric APs depends in part on the phosphoinositides found in the relevant membrane compartments (6–8). PI-4-P is the most prevalent phosphoinositide in the TGN, and AP-1 recruitment to the TGN requires a lipid kinase that phosphorylates phosphatidylinositol at position 4 (8), as well as the small GTPase, Arf1 (9, 10). Thus, AP-1 may recognize the combined presence of Arf1 and PI-4-P or related lipids (11, 12). The structure of the AP-2 core reveals a site near the N terminus of the α chain that could determine the interaction of AP complexes with phosphoinositides. The AP-2 core crystallizes in the presence of inositol hexaphosphate ($InsP_6$, used as a phosphoinositide mimetic), which creates a lattice contact by bridging one corner of the α chain and a positively charged patch on the μ2 chain of another complex. Intracellular localization experiments with mutated overexpressed α chain suggest that the α-chain site participates in a functional interaction with the headgroup of PI-3,4,5-P3, a component of the plasma membrane (13). Mutational experiments based on the structure also implicate the μ2 basic patch in binding to liposomes bearing PI-4,5-P2 and to the plasma membrane (14), but μ1 lacks this concentration of positive charge.

The AP-2 core structure poses several functional questions. Is the observed structure indeed a defined inactive conformation? Can we use information from the structure to confirm or modify the notion that a particular site on one of the large chains determines phosphoinositide interaction? We have determined the structure of the homologous core of AP-1. Its overall structure is closely similar to that of the core of AP-2, although their crystal contacts are completely different. The similarity supports the proposal that these core structures represent a defined inactive conformation. The AP-1 core crystals do not contain an inositol phosphate, and the corner of the γ chain that corresponds to the α chain $InsP_6$-binding site differs noticeably from that of its α counterpart. We show that directed mutations of selected residues at this corner interfere with AP-1 recruitment to the TGN and decrease liposome binding of AP-1 cores *in vitro*, but without affecting the interaction of AP-1 with Arf1 complexed to GTPγS. The data suggest that this site helps to determine the association of AP-1 with Arf1-bearing membrane compartments by interacting with negatively charged lipid headgroups like that of PI-4-P.

Materials and Methods

Expression and Purification of Proteins. cDNA-encoding residues 1–584 of rat β1, 1–423 of mouse μ1A, and 1–158 of mouse σ1A

Freely available online through the PNAS open access option.

Abbreviations: TGN, trans-Golgi network; AP, adaptor protein; μ2C, C-terminal domain of the μ2 subunit; μ2N, N-terminal domain of the μ2 subunit; $InsP_6$, inositol hexaphosphate; PS, phosphatidylserine.

Data deposition: The atomic coordinates and structure factors have been deposited in the Protein Data Bank, www.pdb.org (PDB ID code 1W63).

[§]E.M. and J.W. contributed equally to this work.

**To whom correspondence should be addressed. E-mail: harrison@crystal.harvard.edu.

adaptins were each subcloned into pFastBac1 vectors; cDNA encoding residues 1–613 of mouse γ-adaptin was subcloned into a pFastBacHTb vector. Recombinant baculoviruses were generated with the Bac-to-Bac baculovirus expression system (BD Biosciences). The heterotetrameric complex of AP-1 core was expressed by coinfection of Hi5 cells with all four recombinant baculoviruses. Details of the purification are provided as *Supporting Text*, which is published as supporting information on the PNAS web site. The pure AP-1 cores were concentrated to between 30 and 40 μM in 20 mM Tris·HCl/100 mM NaCl/2 mM 2-mercaptoethanol/1 mM EDTA, by using a 50,000 M_r Ultra15 concentrator (Millipore) and samples were stored at 4°C. Myristoylated Arf1 was purified as described (15) after its generation in *Escherichia coli* by coexpression of Arf1 and yeast *N*-myristoyltransferase (16).

Preparation of Vesicles and Lipid-Binding Assay. Combinations of dioleoyl phosphatidylcholine, dipalmitoyl phosphatidylethanolamine, brain phosphatidylserine (PS), and brain PI-4-P (Sigma) (0.5 mg final) were dissolved in a glass tube in 200 μl of chloroform/methanol (2/1). The solvents were removed with a stream of nitrogen followed by overnight exposure to vacuum. The lipids were resuspended by vortex mixing for 20 s at room temperature with 100 μl of Tris buffer (10 mM Tris·HCl, pH 7.5/50 mM NaCl/1 mM DTT) and the vesicles (5 mg/ml) were stored at 4°C and used within 1 week of preparation.

AP-1 cores (0.2 μM) containing the wild type or the γ-adaptin mutants Y45A or R48A were mixed with the vesicles (1 mg/ml) for 15 min at room temperature in a final volume of 75 μl (Tris buffer). The samples were then subjected to centrifugation for 10 min at 200,000 ×*g* at 25°C (TL100, Beckman Coulter) and the supernatants were removed. The pellets were resuspended with 30 μl of Tris buffer and supernatants and pellets were subjected to SDS/PAGE, Coomassie blue staining, and densitometry. Myristoylated Arf1 (myrArf1) (8 μM dissolved in Tris buffer containing 1 mM $MgCl_2$ and 2 mM EDTA) was preloaded with GTPγS (40 μM) for 45 min at 37°C. Vesicles containing myrArf1/GTPγS were centrifuged, resuspended in Tris buffer supplemented with 1 mM $MgCl_2$, and used for AP-1 binding as described above.

Crystallization and Diffraction Data Collection. Crystals were grown at 4°C by hanging-drop vapor diffusion against reservoirs containing 8–9% ethanol/0.1 M Na Hepes, pH 7.5/2 mM cysteine. Crystals appeared after 1–3 weeks and grew to their final dimensions (100 × 100 × 30 μm) in 3–5 weeks. The primitive hexagonal cell had dimensions a = b = 178 Å, and c = 1,135 Å.

For data collection, the mother liquor in the drop was substituted with 10% 2-methyl-2,4-pentanediol (MPD)/0.1 M Na Hepes, pH 7.5/0.1 M NaCl/2 mM cysteine; the crystals were then transferred briefly into 27% MPD/0.1 M Na Hepes, pH 7.5/0.1 M NaCl/0.2 mM cysteine and plunged into liquid N_2. Data were collected at 100 K at the F1 beamline of the Cornell High Energy Synchrotron Source (Ithaca, NY). The long c cell edge dictated the data collection strategy. An 80-μm collimated beam and a 900-mm crystal-to-detector distance were used to achieve adequate spot separation. Low-resolution datasets (40–7.5 Å) were collected by using a single 2 × 2 charge-coupled device (CCD) detector. High-resolution datasets (20–4.0 Å) were collected by using two vertically mounted 2 × 2 CCD detectors. Because of spot overlap, data were recorded in 0.4° and 0.2° wedges; starting perpendicular to c, 25°–30° were recorded with 0.4° frames, and the rest, with 0.2° frames. The data were processed in space group $P3_112$ with DENZO and scaled with SCALEPACK (17). Two low- and 10 high-resolution datasets, or 1,505 frames, contributed to the final merged data (Table 1, which is published as supporting information on the PNAS web site).

Structure Determination and Refinement. Molecular replacement, as implemented in AMORE (18), used the entire AP-2 core as a search model and data in the 25- to 7-Å resolution range. The rotation search yielded three top solutions, just above background. In the translation search, both $P3_212$ and $P3_112$ were tested, but only the former yielded a correct solution. Each rotation solution gave two translation solutions, indicating the presence of six core complexes in the asymmetric unit. Rigid body refinement in AMORE resulted in R = 47.1% and correlation coefficient = 56.1.

For refinement, 5% of the data, in thin-resolution shells, was set aside for crossvalidation (19). For rigid-body refinement with data from 40- to 4-Å resolution, each subunit was a rigid body, except for μ1, which was divided into N and C domains, making a total of 30 rigid bodies per asymmetric unit. R_{free} was 48.8% at the end of this stage. We determined noncrystallographic symmetry operators and carried out 6-fold averaging combined with histogram-matching and solvent-flattening (65% solvent), by using DM (20) with no phase combination at the end of each cycle. The $2F_o-F_c$ SIGMA-A weighted electron density map (21) was readily interpretable. Model rebuilding was done with O (22). Data from 40- to 4-Å resolution were used to refine a thermal parameter for each domain, followed by gradient minimization, torsion-angle simulated annealing, further gradient minimization, and group thermal parameter refinement, all as implemented in CNS (23). Hydrogen bonds in all α-helices were tightly restrained. Multiple rounds of alternating refinement and rebuilding decreased R to 29.7% and R_{free} to 31.0%. The final model lacks residues 590–613 of γ; 1, 268–274, and 584 of β1; 1, 146–156, 219–231, and 363–372 of μ1; and 149–158 of σ1. Relevant crystallographic statistics are in Table 1. Figures were prepared with the programs MOLSCRIPT (24), ALSCRIPT (25), O (22), RASTER3D (26), and SPOCK (http://mackerel.tamu.edu/spock/Manual/Manual/Manual.html).

Results and Discussion

Structural Overview. The trunks of γ and β1, like those of α and β2, are composed almost entirely of α-zigzags (14 each) of the type known as "HEAT repeats" (Fig. 1*a*). The twist of the HEAT-repeat elements imparts to each of the large-chain trunks the shape of a boomerang, with curved arms of unequal length. The two subunits interlink through contacts at their extremities, forming a hollow lozenge-like basket (Fig. 1 *b* and *c*). Because γ and β1 have closely related folded structures, the basket has a pseudo-2-fold axis. The σ1 subunit and the N-terminal domain of the μ1 subunit (μ1N), which are structurally similar, dock within the angular bends of γ and β1, respectively. Although σ1 and μ1N have essentially no direct interaction, each contacts the N-terminal part of the large chain that primarily embraces the other. Thus, all four chains may be required for a fully stable assembly, and the two halves (γ-σ1 and β1-μ1) may be only marginally stable on their own.

The patterns of HEAT repeats in the AP-1 large chains follow closely their AP-2 counterparts. One repeat contains ≈38 residues in an α-helical hairpin, so stacked on the adjacent hairpin that the entire array is a right-handed superhelix. The first helix in each repeat is on the outside (convex) surface of the curved stack; the second, on the inside. Both γ and β1 have a discontinuity in the stacking between repeats 5 and 6 and a less marked discontinuity between repeats 11 and 12, and, in both, the stronger stacking discontinuity after repeat 5 creates the apparent right-angle bend. The γ subunit starts with an extra single α-helix, and the polypeptide chain that follows the 14th repeat in each subunit projects back along the stack. Despite their obviously similar architectures, the β1 trunk is more sharply curved than the γ trunk, and the two polypeptides can be superimposed not along their entire length but only a few repeats at a time.

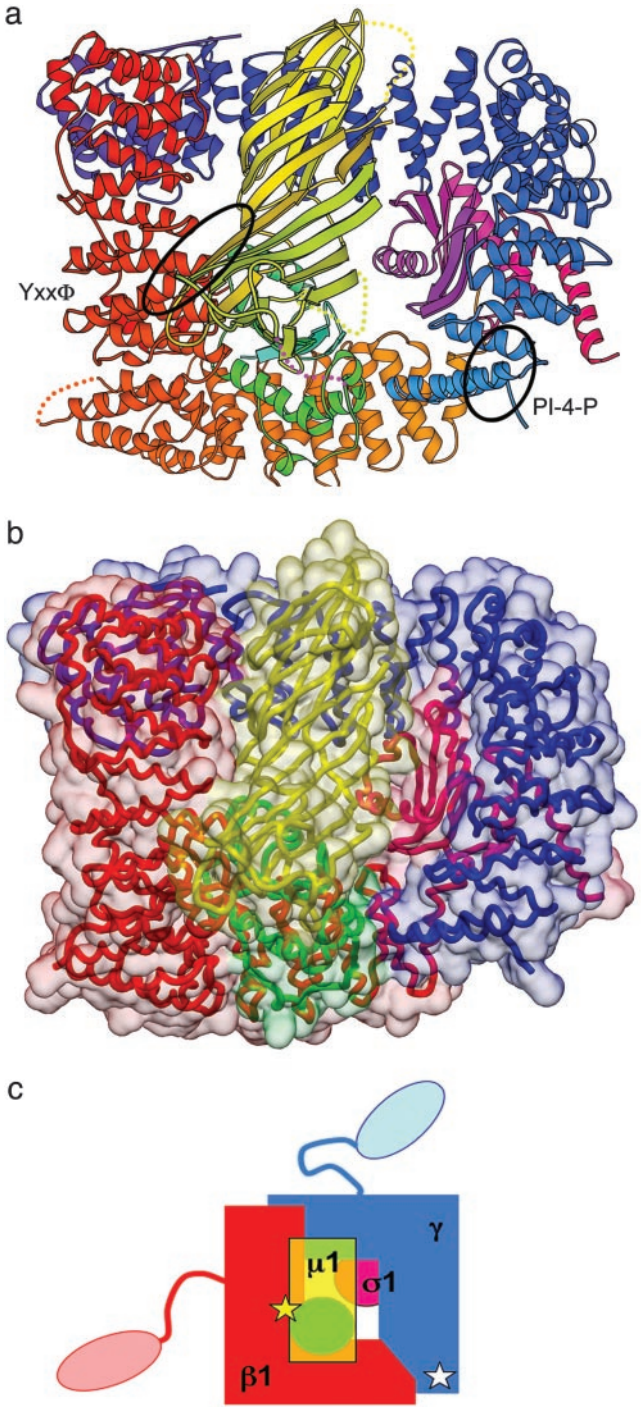

Fig. 1. Structure of the AP-1 core. (*a*) Ribbon representation. The γ chain is blue; β1, red; μ1N, green; μ1C, yellow–orange; and σ1, magenta. Each chain is color-ramped, from the N to the C terminus. The large chains go from a lighter to a darker shade: μ1 goes from green in μ1N to yellow in μ1C. Disordered segments are dotted lines of appropriate color. The disordered connecting link from μ1N to μ1C is a purple dotted line. Locations of the proposed PI-4-P-binding site on γ and of the YxxΦ site on μ1 are shown by black ellipses. A pseudo-2-fold axis, running diagonally from upper left to lower right, relates the two large-chain trunks to each other and μ1N to σ1. (*b*) Molecular surface representation. Colors as in *a*. (*c*) Diagram of AP-1. The drawing applies also to AP-2 (4) and presumably to AP-3 and AP-4 as well. The core comprises the large-chain trunks (γ, blue; β1, red), the medium chain (μ1N, yellow–green; μ1C, yellow–orange), and the small chain (σ1, magenta). The appendages of the large chains are linked to the trunks by extended flexible connectors. Yellow star, binding site for tyrosine-based sorting signal; white star, binding site for inositol-phosphate headgroup (proposed).

As in the AP-2 core, the two distinct domains of μ1 (μ1N and μ1C) are connected by a flexible segment of 20 residues (145–164), which faces one margin of the complex. The elongated μ1C has two similar halves. Each half is a β-sandwich with four strands on each face. The side that faces outward in the first half is the counterpart of the side that faces inward in the second half, and the two halves are related by a pseudo-2-fold screw axis approximately parallel to the direction of the strands. A final C-terminal strand runs between the two outward-facing sides and creates a continuous nine-strand sheet.

As anticipated from the high degree of sequence identity among corresponding subunits, AP-1 and AP-2 have very similar structures. The β1 and β2 trunks superpose almost perfectly, because their entire sequences align without any gaps. The helices of the more divergent α and γ trunks also superpose well, but there is some variation in the conformations and lengths of the interhelical loops. One such difference is in the loop between the second and third helices of the subunit, which is the site of interaction with phosphoinositide head groups in α. The μ1 and μ2 subunits have several structural differences that suggest differences in functional specificity, as discussed further below. The σ1 subunit has a 16-residue C-terminal extension relative to σ2. Seven of these residues (142–148) are part of a C-terminal α-helix; the last nine are disordered.

The AP-1 complexes pack in the crystals in helical stacks, with three complexes per turn. These stacks run from one unit cell to the next, perpendicular to the crystallographic 3-fold screw axis (Fig. 5*a*, which is published as supporting information on the PNAS web site). There are two crystallographically independent stacks of this sort, which cross at an angle of 110°. The coherence of each helical stack is determined by an interface (2,100 Å^2 of buried area) that includes the concave surface of μ1C on one side and parts of β1, γ, and σ1 on the other (Fig. 5*b*). There is no known intracellular role for a stacking of this sort, but the interaction seen in the crystal illustrates that the extended concave surface of μC may have functional significance for interactions with other proteins beyond the limited contact site it provides for YppΦ motifs at one edge of its nine-strand sheet.

Sorting-Signal Binding and Conformational Change. AP-1, like AP-2, recognizes peptides with a YppΦ consensus motif (1, 2). The location of the binding site on μ2 for such peptides was first revealed by crystal structures of isolated μ2C bound to two different sorting peptides [ref. 5; see also Protein Data Bank (PDB) ID codes 1H6E, 1HES, and 1I31]. The peptide straddles one edge of the nine-strand sheet, bracketing the C-terminal strand (Fig. 1*a*). There is a pocket for the tyrosine side chain on the surface of the sheet facing outward in the complex and a second pocket for the bulky hydrophobic side chain at Y + 3, on the inward-facing side of the sheet. The latter pocket is occupied, in both the AP-1 and AP-2 complexes by a hydrophobic residue from the β chain (βVal-365) at the tip of one of the HEAT repeat zigzags (Fig. 1*a*). The μ chain must therefore shift away from β to accommodate the sorting-signal peptide.

There are subtle specificity differences between AP-1 and AP-2 for residues other than the tyrosine and the large hydrophobic (1, 2, 27). Endocytic sorting signals best recognized by μ2 tend to have a positively charged residue at positions Y + 1 or Y + 2, whereas no such preference has been noticed in the signals recognized by μ1. The structures of μ1 and μ2 are so similar in the vicinity of the peptide-binding site, however, that it is difficult to rationalize any of the apparent distinctions.

The similar positions of the μ chains in AP-1 and AP-2, neatly docked into the large-chain "basket," and the insertion of a β chain hydrophobic residue into the Y + 3 pocket provide strong evidence that the crystal structures represent functionally significant closed states of the adaptor complexes. It is clear that the conformation of the adaptors is essentially unaffected by crystal

contacts, because the molecular packing in our AP-1 crystals is completely unrelated to that in the AP-2 crystals (4).

Collins *et al.* (4) have proposed a specific model for how μ2C might swing away from the α:β2 base against which it docks to open the site for YppΦ interaction. By assuming membrane-headgroup contacts for both the helix-2/helix-3 corner of the α chain and the positively charged patch on μ2 and by requiring that the YppΦ-binding site approach the membrane as well (these sorting signals can be quite close to the transmembrane segment of a receptor), they arrive at a picture in which μ2C rotates by ≈90° (forward and top edge down in the view in Fig. 1) so that its extended surface lies against the membrane. Because the positively charged patch is absent in μ1, we can entertain models with quite different displacements and rotations of μC (for example, forward and counterclockwise in Fig. 1), bringing the edge of μC that contacts the sorting signal toward the membrane.

There are some additional constraints on models for the open state of the core. Phosphorylation of a threonine residue in the linker between μ-chain domains (μ2Thr-156, corresponding to μ1Thr-154) enhances affinity for YppΦ sorting signals (28, 29). Coassembly of intact AP complexes with clathrin into coats *in vitro* likewise enhances their affinity for YppΦ sorting signals, and the μ subunit becomes susceptible to a specific trypsin cleavage (30). Similarly, AP-1 bound to Golgi membranes undergoes a conformational change revealed by increased sensitivity of μ1 to trypsin (28). By combining information about the sequence at the μ2 cleavage site (31) with knowledge of the μ2 structure, we can identify the protease-sensitive segment as a disordered loop around residue 224 (not, as one might have expected, the interdomain linker). The same loop is present and disordered in μ1. In the AP-1 and AP-2 core structures, this loop is on the "underside" of the μ-chain C-terminal domain, protected from protease attack. When clathrin binding activates the complex, μC evidently swings far enough from the large-chain pedestal to admit a protease. This observation implies that the shift is a substantial one, perhaps even with the μC domain "floating freely" on the 10- to 15-residue linker segment, so that it can locate sorting signals in diverse positions with respect to the membrane (32).

Clathrin associates through its terminal domain with the β-chain hinge of AP-1 through AP-3 (33, 34). How this interaction might induce or stabilize a conformational change remains an open question. One possibility is that one of the large-chain appendage domains binds back to the core, and that clathrin releases this potential autoregulation when it associates with the hinge. Another is that the clathrin terminal domain, once bound to the β-chain hinge of the adaptor complex, interacts with the core in some additional way.

Potential Phosphoinositide-Binding Site. We have not been able to obtain complexes by soaking the crystals with any of a variety of potential phosphoinositide or inositol phosphate ligands or by cocrystallization, but we can deduce aspects of a potential interaction with PI-4-P or PI-4,5-P2 (8, 11) by reference to the $InsP_6$ site in the AP-2 crystals, where the ligand required for crystallization lies at a molecular contact (4). One face of that contact is a notch created by helices 2 and 3 of the α subunit and by the loop connecting them. The other face is a positively charged patch on μ2C not conserved in μ1. Residues in the α subunit that contact $InsP_6$ include αArg-11, αLys-43, αTyr-53, αLys-57, αTyr-58, and αLys-61, as well as the backbone amide of αGly-12. A triple mutation of Lys-55, -56, and -57 to Gln prevents recruitment to plasma membrane-coated pits and overexpression of the mutant inhibits plasma membrane localization of AP-2, presumably by displacing the endogenous wild-type α chain (35). Thus, there is evidence that the α-chain site is indeed important for membrane association. Of the residues that contact $InsP_6$ in the AP-2 crystals, only αLys-57 and -61 are conserved in the γ subunit as γArg-48 and γLys-52, and the overall charge density in the region is lower, consistent with preference for a phosphoinositide with one rather than two or three phosphates. The notch between helices 2 and 3 of the γ chain is partly blocked by residues γMet-1 to γArg-6 at its N terminus, which takes a different course in our structure than the corresponding part of the α chain in AP-2 (Fig. 2). These residues would need to shift aside to admit a head group to the putative binding notch. Their conformation might account for the failure of our soaking experiments to yield detectable occupancy.

Inspection of the corner between helices 2 and 3 suggested to us that γTyr-45, γArg-48, and γLys-52 would be good candidates

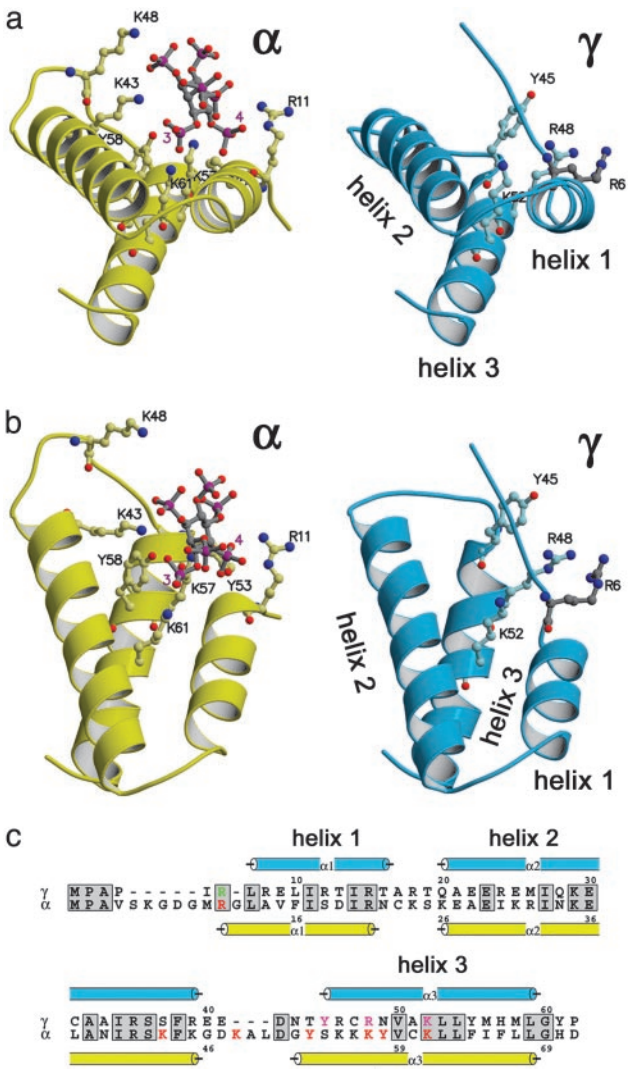

Fig. 2. Comparison of the helix 2–helix 3 corner in the α chain (*Left*) of AP-2 and the γ chain (*Right*) of AP-1. (*a*) View as if looking from the left in Fig. 1*a* toward the corner enclosed in the oval; the top of the present figure corresponds to the bottom of Fig. 1. (*b*) The same as *a*, but rotated by 90° as shown. The α-adaptin of AP-2 is in yellow; the γ-adaptin of AP-1 is in cyan. The $InsP_6$ molecule and residues involved in binding phosphoinositides are in ball-and-stick representation (nitrogen, blue; oxygen, red; phosphorus, magenta; carbon, pale yellow in AP-2, pale cyan and gray in AP-1, and gray in $InsP_6$). (*c*) Amino acid sequences in this region and their secondary structures. The secondary-structure symbols are colored to match the ribbon diagram. Residues involved in phosphoinositide binding are in magenta (γ chain) and red (α chain); the residue R6 of γ chain is in green.

CELL BIOLOGY

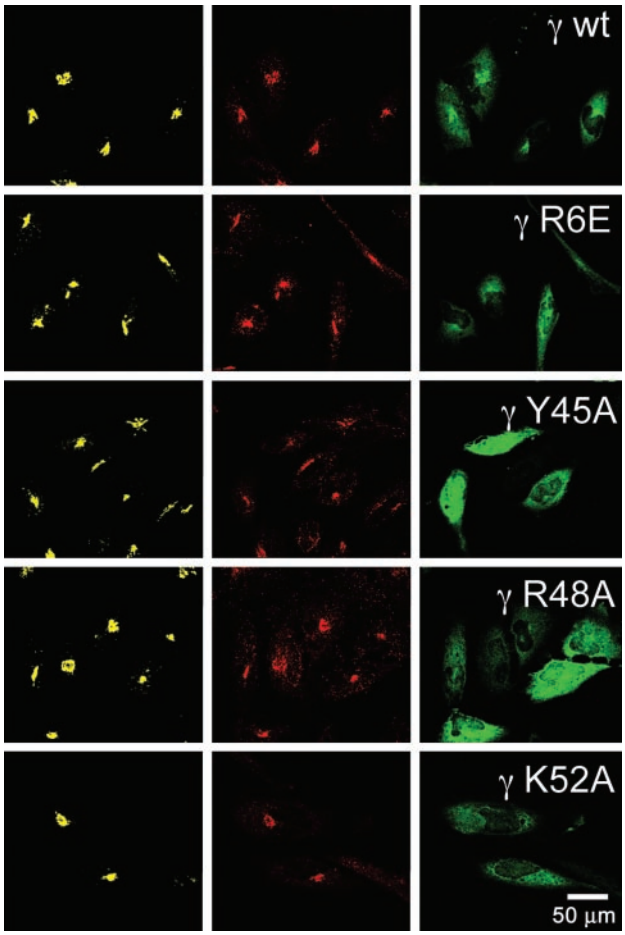

Fig. 3. Effect of mutations in γ chain on the intracellular distribution of AP-1. HeLa cells transiently expressing wild-type or mutant (R6E, Y45A, R48A, and K52A) mouse γ-adaptin fused to enhanced GFP (green, *Right*) were fixed and fluorescently labeled with a sheep polyclonal antibody to TGN46 (yellow, *Left*) or a mouse monoclonal antibody 100/3 to human (but not mouse) γ-adaptin (endogenous γ; red, *Center*).

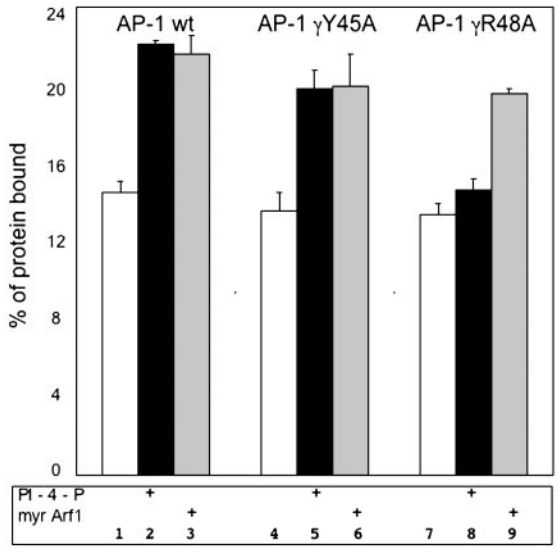

Fig. 4. Effect of mutations in γ chain on recruitment of AP-1 cores to liposomes. AP-1 cores (0.2 μM) containing either wild-type or mutant (Y45A or R48A) mouse γ subunits were incubated with liposomes and the amount bound was determined as described in *Materials and Methods*. The composition of the liposomes (mol %) was 57% phosphatidylcholine (PC), 28% phosphatidylethanolamine (PE), and 15% PS (lanes 1, 3, 4, 6, 7, and 9) or 57% PC, 28% PE, 10% PS, and 5% PI-4-P (lanes 2, 5, and 8). Myristoylated Arf1, preloaded with GTPγS, was included in the liposomes analyzed in lanes 3, 6, and 9. Histograms show the amount (average ± standard deviation from three to four experiments) of AP-1 core cosedimented with liposomes (expressed as percent of total). In the absence of liposomes or the presence of liposomes containing PC and PE only, the amount of AP-1 in the pellet was <1–2%.

for phosphoinositide head-group contacts (Fig. 2). We mutated each of these residues to Ala and asked whether the changes affect TGN targeting of the modified AP-1 complex. We also included Arg-6 in this series of mutations to examine a possible role for the N-terminal segment.

To study the effects of these mutations, we transfected HeLa cells with constructs encoding wild-type and mutant AP-1 γ chain tagged with enhanced GFP (EGFP). We confirmed, as reported (36), that most of the EGFP-tagged wild-type γ concentrates in the perinuclear area, with the remainder in more peripheral sites (Fig. 3 *Top*). We also confirmed that reduction of phosphatidylinositol-4-kinase IIα by RNA interference prevented this perinuclear localization (data not shown), just as it blocked similar localization of endogenous γ (incorporated into AP-1), detected by immunofluorescence (8). The targeting of the recombinant tagged γ chain is thus just like that of the endogenous protein. The images in Fig. 3 show that mutation of any one of residues 45, 48, or 52 to Ala in γ-adaptin prevents normal perinuclear targeting, but that mutation of Arg 6 to Glu, which projects away from the proposed site for PI-4-P, has no effect. The integrity of the TGN and Golgi compartments was maintained in these experiments, because expression of the mutant proteins did not affect targeting of the TGN marker TGN46 (Fig. 3) or β-COPI (a marker for the Golgi compartments; data not shown). Expression in insect cells of any of these mutated γ chains together with the other three chains of AP-1 yielded assembled complexes with native-like properties (Fig. 6, which is published as supporting information on the PNAS web site), showing that the mutant γ subunits incorporate normally into AP-1, and that failure of TGN targeting is not a consequence of reduced complex formation.

Because recruitment of AP-1 to Golgi membranes depends not only on active phosphatidylinositol-4-kinase IIα but also on the small GTPase Arf1 in its GTP-bound state (9, 10), we examined the effects of two of the γ chain mutations on the association of recombinant AP-1 cores with liposomes containing Arf1 or PI-4-P. As expected, myristoylated Arf1 activated by binding of GTPγS enhanced association of wild-type AP-1 core with liposomes containing PS (12). AP-1 cores containing γ subunits with alanine substituted for Y45 or R48 responded similarly (Fig. 3). We conclude that these mutations do not affect a critical Arf1-binding interface. Incorporation of PI-4-P into the PS-containing liposomes also enhanced AP-1 association, establishing that AP-1 interacts with PI-4-P.

The R48A mutation eliminated the PI-4-P enhancement of AP-1 recruitment to liposomes, but it did not impair background interaction with PS (Fig. 4). Thus, the loss of a positive charge alters specificity but does not destroy affinity for negatively charged lipids generally. We propose that R48 is important for Golgi targeting because of its interaction with PI-4-P, and that in the absence of this contact, Arf1 does not suffice. It is remarkable that despite the extensive network of parallel interactions in which the nearly 300-kDa AP-1 complex participates, a single point mutation at a lipid–head-group interaction site is sufficient to disrupt correct intracellular localization.

The Y45A mutation also disrupts localization, but it does not affect PI-4-P or Arf1 enhancement in our liposome-binding assay. We cannot resolve here the difference in apparent behavior. It is possible that there are subtle changes in affinity that

are not detected by the *in vitro* assay. In some of our intracellular localization experiments, it appeared that this mutation might have a weaker effect that R48A, but we have not yet established a firm correlation.

In its requirement for both a small GTPase and a phosphoinositide, AP-1 resembles a number of other proteins that are recruited to specific intracellular membrane compartments. Examples include OSBP and FAPP1, which recognize the presence of Arf1 and PI-4-P in the TGN (37, 38). The structural basis of stereochemical specificity for a particular headgroup geometry has been difficult to demonstrate, however. As with AP-2, structures have been determined for domains from AP-180 and epsin proteins in complex with $InsP_6$ (39, 40) but not for complexes with the headgroups they are thought to recognize. A survey of the 33 pleckstrin homology domains from yeast found that only one had clear *in vitro* specificity for a defined phosphoinositide (41). Thus, we cannot rule out an indirect correlation between particular members of the heterotetrameric AP family and the phosphoinositide content of the membranes to which they localize in a cell.

Metabolism of lipids in general, and of phosphoinositides in particular, is under tight temporal and spatial control. One form of membrane identity seems to be provided by the relative enrichment of specific phosphoinositides in a given membrane (for a recent review, see ref. 42). The properties and structures of AP-1 and AP-2 cores suggest that adaptors, rather than the cargo they sort, are the critical detectors of phosphoinositide content. Their relatively low affinity and modest specificity for particular phosphoinositides can be understood by recognizing that they are coincidence detectors. Thus, AP-1 responds to the combined presence of PI-4-P and Arf1, which draw it to locations where it can then interact with both cargo and clathrin. The structure described here is a step toward rationalizing the properties and intricacies of such networks.

We thank Marian Szebenyi, Mike Cook, and the staff of beamline F1 at the Cornell High Energy Synchrotron Source for assistance with data collection; April Griffin (National Institutes of Health, Bethesda) for help in creating constructs; and Lois E. Greene for the enhanced GFP-γ-adaptin construct. This work was supported by National Institutes of Health Grants GM36548 (to T.K.) and GM066110 (to H.L.Y.) and a Robert A. Welch Foundation grant (to H.L.Y.). S.C.H. is an Investigator with the Howard Hughes Medical Institute.

1. Kirchhausen, T. (1999) *Annu. Rev. Cell Dev. Biol.* **15,** 705–732.
2. Bonifacino, J. S. & Traub, L. M. (2003) *Annu. Rev. Biochem.* **72,** 395–447.
3. Robinson, M. S. (2004) *Trends Cell Biol.* **14,** 167–174.
4. Collins, B. M., McCoy, A. J., Kent, H. M., Evans, P. R. & Owen, D. J. (2002) *Cell* **109,** 523–535.
5. Owen, D. J. & Evans, P. R. (1998) *Science* **282,** 1327–1332.
6. West, M. A., Bright, N. A. & Robinson, M. S. (1997) *J. Cell Biol.* **138,** 1239–1254.
7. Jost, M., Simpson, F., Kavran, J. M., Lemmon, M. A. & Schmid, S. L. (1998) *Curr. Biol.* **8,** 1399–1402.
8. Wang, Y. J., Wang, J., Sun, H. Q., Martinez, M., Sun, Y. X., Macia, E., Kirchhausen, T., Albanesi, J. P., Roth, M. G. & Yin, H. L. (2003) *Cell* **114,** 299–310.
9. Traub, L. M., Ostrom, J. A. & Kornfeld, S. (1993) *J. Cell Biol.* **123,** 561–573.
10. Stamnes, M. A. & Rothman, J. E. (1993) *Cell* **73,** 999–1005.
11. Crottet, P., Meyer, D. M., Rohrer, J. & Spiess, M. (2002) *Mol. Biol. Cell* **13,** 3672–3682.
12. Zhu, Y., Traub, L. M. & Kornfeld, S. (1998) *Mol. Biol. Cell* **9,** 1323–1337.
13. Gaidarov, I., Chen, Q., Falck, J. R., Reddy, K. K. & Keen, J. H. (1996) *J. Biol. Chem.* **271,** 20922–20929.
14. Rohde, G., Wenzel, D. & Haucke, V. (2002) *J. Cell Biol.* **158,** 209–214.
15. Franco, M., Chardin, P., Chabre, M. & Paris, S. (1995) *J. Biol. Chem.* **270,** 1337–1341.
16. Duronio, R. J., Jackson-Machelski, E., Heuckeroth, R. O., Olins, P. O., Devine, C. S., Yonemoto, W., Slice, L. W., Taylor, S. S. & Gordon, J. I. (1990) *Proc. Natl. Acad. Sci. USA* **87,** 1506–1510.
17. Otwinowski, Z. & Minor, W. (1997) in *Methods in Enzymology*, eds. Carter, C. W., Jr., & Sweet, R. M. (Academic, New York), Vol. 276, pp. 307–326.
18. Navaza, J. (2001) *Acta Crystallogr. D* **57,** 1367–1372.
19. Kleywegt, G. J. & Brunger, A. T. (1996) *Structure (Cambridge, U.K.)* **4,** 897–904.
20. Cowtan, K. & Main, P. (1998) *Acta Crystallogr. D* **54,** 487–493.
21. Collaborative Computational Project. (1994) *Acta Crystallogr. D* **50,** 760–763.
22. Jones, T. A., Zou, J. Y., Cowan, S. W. & Kjeldgaard, M. (1991) *Acta Crystallogr. A* **47,** 110–119.
23. Brunger, A. T., Adams, P. D., Clore, G. M., DeLano, W. L., Gros, P., Grosse-Kunstleve, R. W., Jiang, J. S., Kuszewski, J., Nilges, M., Pannu, N. S., *et al.* (1998) *Acta Crystallogr. D* **54,** 905–921.
24. Kraulis, P. J. (1991) *J. Appl. Crystallogr.* **24,** 946–950.
25. Barton, G. J. (1993) *Protein Eng.* **6,** 37–40.
26. Merritt, E. A. & Bacon, D. J. (1997) in *Methods in Enzymology*, eds. Carter, C. W., Jr., & Sweet, R. M. (Academic, New York), Vol. 277, pp. 505–524.
27. Ohno, H., Aguilar, R. C., Yeh, D., Taura, D., Saito, T. & Bonifacino, J. S. (1998) *J. Biol. Chem.* **273,** 25915–25921.
28. Ghosh, P. & Kornfeld, S. (2003) *J. Cell Biol.* **160,** 699–708.
29. Ricotta, D., Conner, S. D., Schmid, S. L., von Figura, K. & Honing, S. (2002) *J. Cell Biol.* **156,** 791–795.
30. Rapoport, I., Miyazaki, M., Boll, W., Duckworth, B., Cantley, L. C., Shoelson, S. & Kirchhausen, T. (1997) *EMBO J.* **16,** 2240–2250.
31. Matsui, W. & Kirchhausen, T. (1990) *Biochemistry* **29,** 10791–10798.
32. Kirchhausen, T. (2002) *Cell* **109,** 413–416.
33. Gallusser, A. & Kirchhausen, T. (1993) *EMBO J.* **12,** 5237–5244.
34. ter Haar, E., Harrison, S. C. & Kirchhausen, T. (2000) *Proc. Natl. Acad. Sci. USA* **97,** 1096–1100.
35. Gaidarov, I. & Keen, J. H. (1999) *J. Cell Biol.* **146,** 755–764.
36. Puertollano, R., van der Wel, N. N., Greene, L. E., Eisenberg, E., Peters, P. J. & Bonifacino, J. S. (2003) *Mol. Biol. Cell* **14,** 1545–1557.
37. Levine, T. P. & Munro, S. (2002) *Curr. Biol.* **12,** 695–704.
38. Godi, A., Di Campli, A., Konstantakopoulos, A., Di Tullio, G., Alessi, D. R., Kular, G. S., Daniele, T., Marra, P., Lucocq, J. M. & De Matteis, M. A. (2004) *Nat. Cell Biol.* **6,** 393–404.
39. Ford, M. G., Mills, I. G., Peter, B. J., Vallis, Y., Praefcke, G. J., Evans, P. R. & McMahon, H. T. (2002) *Nature* **419,** 361–366.
40. Mao, Y., Chen, J., Maynard, J. A., Zhang, B. & Quiocho, F. A. (2001) *Cell* **104,** 433–440.
41. Yu, J. W., Mendrola, J. M., Audhya, A., Singh, S., Keleti, D., DeWald, D. B., Murray, D., Emr, S. D. & Lemmon, M. A. (2004) *Mol. Cell* **13,** 677–688.
42. Munro, S. (2004) *Nat. Cell Biol.* **6,** 469–472.